

# **Ground surface temperature history since the Last Glacial Maximum in Northeast Asia: Reconstructions from the borehole geotherms of the International Continental Scientific Drilling Program**

**Guangzheng Jiang<sup>1,2</sup>, Yuntao Tian<sup>3,4</sup>, Qingtian Lv<sup>5</sup>, Mike Sandiford<sup>6</sup>, Yizuo Shi<sup>7</sup>, Changchun Zou<sup>8</sup>, Feng Ma<sup>8</sup>, Chenglong Deng<sup>10</sup>, Lijuan He<sup>10</sup>, Shengbiao Hu<sup>10</sup>**

<sup>1</sup> State Key Laboratory of Oil and Gas Reservoir Geology and Exploitation, Chengdu University of Technology, Chengdu, China

<sup>2</sup> College of Energy, Chengdu University of Technology, Chengdu, China

<sup>3</sup> Guangdong Provincial Key Laboratory of Geodynamics and Geohazards, School of Earth Sciences and Engineering, Sun Yat-sen University, Zhuhai, China

<sup>4</sup> Southern Marine Science and Engineering Guangdong Laboratory (Zhuhai), Zhuhai, China

<sup>5</sup> China Deep Exploration Center, China Geological Survey & Chinese Academy of Geological Sciences, Beijing, China

<sup>6</sup> School of Earth Sciences, University of Melbourne, Parkville, Victoria, Australia

<sup>7</sup>PetroChina Research Institute of Petroleum Exploration & Development, Beijing, China

<sup>8</sup> China University of Geosciences, Beijing, China

<sup>9</sup> Institute of Hydrogeology and Environmental Geology, Chinese Academy of Geological Science, Shijiazhuang, China

<sup>10</sup> State Key Laboratory of Lithospheric Evolution, Institute of Geology and Geophysics, Chinese Academy of Sciences, Beijing, China

### **Key Points:**

- We report an undisturbed 6100-m continuous heat-flow profile from the scientific drilling project SK-2e
  - The heat-flow profile recorded a 2 K rise of GST in the last five centuries and a 10 K rise since the Last Glacial Maximum
  - A basin-scale comparison reveals localized heat-flow anomalies induced by advective heat in deep and confined high-permeability aquifers

29 **Abstract**

30 Past ground surface temperature, one of the important aspects of paleoclimate reconstructions,  
 31 can be inverted from borehole temperature measurements. Here, we report continuous 6100-m  
 32 temperature logs in the International Continental Scientific Drilling Program SK-2e. We inverted  
 33 the past ground surface temperature changes from upper borehole temperature logging (<600 m).  
 34 Below this depth, localized fluid flow masks the paleoclimate record. Inversions yield an  
 35 approximately 2 K ground surface temperature rise since 0.1-0.6 kiloyear BP and an  
 36 approximately 10 K rise since 20 kiloyear BP. Assuming a  $\pm 5$  K influence from the deep  
 37 groundwater flow, the inverted temperature rise has varied between 8 K and 12 K since 20  
 38 kiloyear BP, which is consistent with previous reports since the Last Glacial Maximum. Our  
 39 results emphasize the potential of borehole heat-flow profiles as a record of climate changes and  
 40 the importance of climate correction for heat-flow determinations.

41 **Plain Language Summary**

42 Temperatures within the shallow boreholes are perturbed by changes in ground surface  
 43 temperature in response to paleoclimate variations and anthropogenic land use. The ground  
 44 surface temperature varies at different time scales, and these variations penetrate different depths  
 45 underground. Thus, the borehole temperatures can be used for reconstructing the history of  
 46 ground surface temperatures. Based on borehole geotherms of the International Continental  
 47 Scientific Drilling Program in Northeast Asia, the past ground surface temperature changes since  
 48 the Last Glacial Maximum were inverted. The results show a ~2 K surface temperature rise  
 49 during 0.1-0.6 kiloyear BP and a ~10 K rise since 20 kiloyear BP, which is consistent with  
 50 previous independent estimates.

51 **1 Introduction**

52 The Earth's temperature field is one of the controlling factors of petrophysical properties,  
 53 such as seismic velocity and rheological strength. Borehole geothermal measurements open a  
 54 window into the thermal regime of deep Earth, allowing extrapolations to heat flow and  
 55 geotherms, with the combination of thermal conductivity and heat production measurements  
 56 (Furlong and Chapman, 2013). Furthermore, the temperatures within the shallow boreholes are  
 57 often perturbed by groundwater movement (Jessop, 1993; Guillou-Frottier et al., 2013) and  
 58 changes in ground surface temperature (GST) induced by paleoclimate variations and  
 59 anthropogenic land use (Gosnold et al., 2011; Majorowicz et al., 2012). Paleoclimatic signatures  
 60 could perturb equilibrium heat flow densities to more than 2 km (Beltrami et al., 2014).  
 61 Therefore, detailed borehole geothermal studies have the potential to provide unique constraints  
 62 on both deep-earth thermal processes and GST changes.

63 Available global heat-flow and paleoclimate studies primarily rely on shallow (<1000 m)  
 64 boreholes (Huang et al., 2000; Davies, 2013; Cuesta-Valero et al., 2021). Long-term climate  
 65 changes cause significant perturbations in the measured heat flow, leading to deviations in the  
 66 global heat-flow dataset. Climatic perturbations, which are considered noise to determine the  
 67 heat flow, can be used for GST reconstruction (Bodri and Cermak, 2011). The theories and  
 68 technologies for reconstructing the paleoclimate based on borehole temperature have been  
 69 developed (Huang et al., 2000; Davies, 2013; Cuesta-Valero et al., 2021). However, GST  
 70 reconstructions using this method remain limited. Only dozens of the global dataset, including  
 71 70000 borehole temperature logs, have been successfully utilized. One of the primary reasons is

72 that the borehole temperature is inevitably influenced in part by groundwater activities  
 73 (Mottaghy et al., 2005; Jiang et al., 2016). Additionally, vertical distributions of heat production  
 74 are often estimated by empirical correlations between heat production and the rock type, with  
 75 limited constraints from measurements. Superdeep continental scientific drilling boreholes are  
 76 excellent opportunities to constrain the lithospheric thermal structure and to explicitly establish  
 77 the relationship between heat-production variation and depth.

78 The SK-2e borehole is the current deepest scientific drilling project in Northeast Asia,  
 79 with a depth of 7018 m, from which continuous 4134 m cores have been recovered. The SK-2e is  
 80 located in the Songliao Basin, Northeast China, approximately 1200 km west of the Pacific  
 81 subduction zone (Figure 1a). This superdeep scientific drilling provides unique geothermal  
 82 information on the inner Earth's temperature, heat flow, and thermal structure. Moreover, it is  
 83 also valuable in reconstructing past GST changes in Northeast Asia. This paper reports the 6400-  
 84 m continuous temperature logging, thermal conductivity, heat production, and vertical heat-flow  
 85 profile from SK-2e. We also interpret the heat-flow variations in terms of the GST history and  
 86 groundwater movement.

## 87 2 Study site

88 The Songliao Basin, where the SK-2e borehole was targeted, formed on the pre-Triassic  
 89 basement and experienced three filling stages of the syn-rift (150–105 Ma), post-rift (105–79.1  
 90 Ma,) and structural inversion (79.1–64 Ma), with sedimentary thickness up to 6 km (Wang et al.,  
 91 2013; Wang et al., 2016). The basin includes five subunits, including Western Slope, Central  
 92 Depression (where SK-2e is located), Northern Plunge, Southeastern Uplift, and Southwestern  
 93 Uplift (Figure 1b).

94 The previous heat flow data show that the basin is characterized by high heat flow, with a  
 95 mean of  $70.9 \pm 14.4 \text{ mW m}^{-2}$  (Wu and Xie, 1985; Shi et al., 2018). The estimated vertical heat-  
 96 flow profiles exhibit a gradually increasing trend from 0 to approximately 1000 m and positive  
 97 anomalies from 1000 to 2000 m. A purely conductive heat flow cannot explain the observed  
 98 anomalous heat-flow trends. Besides, as shown in Figure 1c, the anomalies coincide distinctly  
 99 with the high-porosity/permeability hydrocarbon reservoirs between the lower K<sub>2n</sub> to the upper  
 100 K<sub>2q</sub> (Wang et al., 2013), suggesting that they stem from advective heat transport associated with  
 101 fluid migration. Significant vertical components or horizontal fluid movements in the inclined  
 102 layer could exist in these high-porosity/permeability zones. Horizontal flow in deep confined  
 103 aquifers is likely to be eastward in the Songliao Basin as the elevation of the western margin is  
 104 approximately 900–1200 m higher than the eastern, leading to correspondingly higher hydraulic  
 105 heads (Zhu, 2011). Furthermore, previously published data indicate an increasing trend of heat  
 106 flow from west to east, with values increasing from 44.4 to 95.0 mW m<sup>-2</sup> (Wu and Xie, 1985).  
 107 This trend further supports a regional aquifer signal consisting of eastward-directed flow. The  
 108 westerly boreholes (e.g., S2 and K2) exhibit the lowest heat-flow values, while higher heat-flow  
 109 values are observed in boreholes G507, TS1, Z12, and X4 located in the central basin, where the  
 110 aquifers extend to deeper levels. The fact that the heat flow anomalies have a wide depth range  
 111 and continuous variation suggests that they are stable and long-lasting over periods of at least ten  
 112 thousand years. Although the contribution of the advective heat transport within aquifers is not  
 113 yet quantitatively resolved, this finding suggests supports the feasibility of GST reconstruction  
 114 from a borehole with a local thermal anomaly. Finally, marking the start of the post-rift thermal  
 115 subsidence phase of the Songliao Basin, K<sub>2q</sub> and the upper strata are unaffected by syn-

116 depositional faulting (Wang et al., 2013), mitigating against the influence of vertical fluid  
 117 migration (Figure 1c). Thus, SK-2e is of great significance in reconstructing the GST and  
 118 confirming basin-scale fluid migration.

### 119 **3 Data collection and observations**

#### 120 **3.1 Temperature logging**

121 The temperature logging of the SK-2e borehole was conducted on March 25, 2016, and  
 122 August 7, 2019. During the second set of measurements, the temperature sensor reached only  
 123 6130 m due to mud obstacles in the lowest section of the borehole. Borehole temperature logging  
 124 was performed using a PPS71 geothermal memory tool, equipped with a platinum resistance  
 125 temperature sensor (maximum temperature: 350 °C) and a 10000-m-long cable. The system  
 126 allows temperature recordings with a 0.01 K sensitivity, a 0.2 K accuracy, and less than 2 s  
 127 response time. The recording time interval was 0.5 s, and a downward logging speed of 6 m/min  
 128 was adopted to ensure sufficient time for the sensor to record the temperature without delay.

129 The first temperature log was recorded 35 days after drilling to a depth of approximately  
 130 4200 m, and the second log was recorded 507 days after drilling had finished, at a depth of 7018  
 131 m. The repeated loggings indicate a distinct thermal recovery process, with the recovered  
 132 temperatures of the two logs crossing at approximately 1400 m. The second temperature log  
 133 records an average temperature gradient of  $36.0 \text{ mK m}^{-1}$  compared with  $31.1 \text{ mK m}^{-1}$  in the first  
 134 log. To assess the temperature recovery, we compare the measured temperatures with the values  
 135 collected from drill stem tests (DSTs), which are widely used in the oil industry to estimate  
 136 equilibrium temperatures. We note that the second temperature log is generally consistent with  
 137 the DST temperature estimates (see Figure 2a), giving confidence that it approximates the  
 138 steady-state temperature profile.

139 The second log shows the temperature abruptly decreases from 17.2 to 8 °C in the  
 140 uppermost 13.6 m, which is consistent with seasonal and annual temperature GST variabilities  
 141 expected for mid-late summer logging. At depths greater than 20 m, the temperature  
 142 continuously increases to 205 °C at 6130 m. The 20-m interval-averaged temperature gradient  
 143 varies between  $10.9 \text{ mK m}^{-1}$  and  $74.4 \text{ mK m}^{-1}$  with distinct peaks at depths of approximately 1200 and  
 144 1600 m. In the shallowest 1000 m, the gradient increases with depth, most prominently in the  
 145 first 120 m and between 860 and 1000 m. Near the surface (20–120 m), the temperature gradient  
 146 is as low as  $16.7 \pm 3.5 \text{ mK m}^{-1}$ . Between 120–860 m, it averages  $30.4 \pm 7.7 \text{ mK m}^{-1}$ . Four apparent  
 147 positive temperature gradient anomalies can be distinguished in Figure 2b.

#### 148 **3.2 Thermal conductivity and heat flow**

149 Thermal conductivity measurements were performed on samples collected from the SK-  
 150 2e ( $n=404$ ) and adjacent boreholes SK-1n ( $n=148$ ) and N2 ( $n=11$ ). Because cores were not  
 151 recovered during drilling for the upper section (less than 2800 m) of the SK-2e borehole, samples  
 152 from the adjacent borehole SK-1n (~60 km west of SK-2e and 0–2000 m continuous cores) and  
 153 N2 (~150 km southwest of SK-2e) were collected to complement the dataset. The thermal  
 154 conductivity was measured by a high-precision non-contact optical scanning technology (Popov  
 155 et al., 1999). Measurements were performed on dry cores along a scanning line on a diametral  
 156 plane at ambient temperature. The measured values were corrected to the in situ conditions  
 157 through water-saturated (porosity) (Beardsmore et al., 2001) and temperature corrections

158 (Sekiguchi, 1984). The porosity was obtained from the neutron log (Chen, 2018; Zou et al.,  
 159 2018). A pressure correction was neglected because the maximum thermal conductivity increase  
 160 remains within 1.3%, according to Kappelmeyer and Haenel (1974).

161 Below 2800 m, the in-situ thermal conductivity is adopted. Above 2800 m, the thermal  
 162 conductivity is referred to as the average value of the SK-1n and N2 for the corresponding  
 163 formations (i.e., K<sub>2q</sub> to Q, as illustrated by the stepped lines in Figure 3a). The measured thermal  
 164 conductivity values range from 2.24 to 3.56 W m<sup>-1</sup> K<sup>-1</sup> and exhibit a slightly increasing trend  
 165 with the depth (Figure 3a). Water-saturated correction of thermal conductivity is essential for the  
 166 samples from the shallow high-porosity stratum, with a maximum correction as high as 40%.  
 167 The porosity decreases to ~2% at the bottom of the hole, where the water-saturated effect  
 168 decreases to less than 1%. The maximum temperature correction of thermal conductivity is about  
 169 -18% at the maximum measured depth of 6100 m (205 °C). The measured and fully corrected  
 170 profiles are shown in Figure 3a. The fully corrected thermal conductivity tends to increase with  
 171 depth in the interval of 0-2000 m and stabilizes thereafter due to the combined effects of  
 172 declining porosity and increasing temperature.

173 The heat flow was calculated as the product of the least squares smoothed temperature  
 174 gradient and the thermal conductivity, derived at approximately 20-m depth intervals, as shown  
 175 in Figures 2c and 3e. The vertical heat-flow values range from 18 to 170 mW m<sup>-2</sup>, with moving  
 176 average estimates mostly in the range of 50-80 mW m<sup>-2</sup>. An increasing trend is observed in the  
 177 shallower section of the borehole, and a gradually decreasing trend occurs in the deeper section.  
 178 The heat flow increases from approximately 28-32 mW m<sup>-2</sup> in the uppermost 120 m to 45-60  
 179 mW m<sup>-2</sup> in the 120-860 m interval and then rises to 110-120 mW m<sup>-2</sup> from 860-1600 m. Below  
 180 this depth interval, the heat flow gradually decreases to 65 mW m<sup>-2</sup> at a depth of ~3340 m. The  
 181 depth interval of 3340-3920 m reveals an apparent anomaly with a magnitude of 86 mW m<sup>-2</sup>.  
 182 Below 4000 m, the heat flow exhibits more minor fluctuations and relatively constant heat flow,  
 183 with an average of 66 mW m<sup>-2</sup>.

### 184 3.3 Heat production

185 The heat-production value is calculated through the empirical equation (Birch, 1954):

$$186 A = 10^{-5} \rho (9.52C_U + 2.56C_{Th} + 3.48C_K) \quad (1)$$

187 where  $A$  is the heat production in  $\mu\text{W m}^{-3}$ ;  $\rho$  is the density in  $\text{kg m}^{-3}$ ;  $C_U$  and  $C_{Th}$  are the U and Th  
 188 concentrations; respectively, in ppm, and  $C_k$  is the K content as a percentage. The uranium and  
 189 thorium concentrations were acquired through inductively coupled plasma mass spectrometry,  
 190 and the potassium concentration was determined by X-ray fluorescence spectroscopy. The  
 191 density was obtained from the neutron log (Chen, 2018; Zou and Zhang et al., 2018). The U, Th,  
 192 and K concentrations in 158 core samples were measured from 2800 m to the bottom at depth  
 193 intervals of 20-50 m.

194 The vertical variations in the U, Th, and K concentrations and heat production with depth  
 195 are shown in Figure 3b-c. Overall, the samples show relatively low U, Th, and K concentrations,  
 196 with a high Th/U ratio, with a mean of  $4.3 \pm 2.8$ , which is much greater than the global mean of  
 197 2.5. The heat production values estimated from the U, Th, and K concentrations are also low  
 198 (sandstones:  $0.75 \pm 0.31 \mu\text{W m}^{-3}$ ; mudstones:  $0.81 \pm 0.36 \mu\text{W m}^{-3}$ ; volcanic rocks:  $0.75 \pm 0.29 \mu\text{W}$   
 199  $\text{m}^{-3}$ ; and metamorphic rocks:  $0.76 \pm 0.18 \mu\text{W m}^{-3}$ ). No distinct differences in the concentrations of  
 200 the radiogenic elements, heat production, or Th/U ratio are observed among rock types (Figure

201 3c). The integrated heat production contribution in the upper 6000-m sedimentary cover is  
 202 equivalent to  $\sim 5 \text{ mW m}^{-2}$  in heat-flow terms. The characteristic heat-flow value of  $66 \text{ mW m}^{-2}$   
 203 obtained in the deepest borehole section yields an equilibrium surface heat value of  $71 \text{ mW m}^{-2}$   
 204 after the heat production contribution is taken into account.

## 205 4 GST inversion method and input data

206 Given the similar lithology and rock properties throughout the SK-2e borehole (Figures  
 207 3d and 3f), the lower heat flow ( $28\text{-}60 \text{ mW m}^{-2}$ ) in the upper 860 m than the deeper sections  
 208 (Figures 2c and 3e) probably implies a significant perturbation from equilibrium, likely due to  
 209 GST changes, which are explored in the section below.

### 210 4.1 Methodology

211 The forward model of borehole climate reconstruction is based on pure conductive heat  
 212 transfer in a homogeneous semi-infinite half-space porous medium. We use finite difference  
 213 techniques to solve the 1-D time-dependent heat conduction equation (2), with the up ( $z=z_0$ )  
 214 temperature boundary ( $T_{GS}$ ) and bottom ( $z=z_{max}$ ) constant heat flow boundary conditions set as  
 215 equations (3) and (4), respectively.

$$216 (\rho c)_e \frac{\partial T}{\partial t} + \frac{\partial}{\partial z} \left( \lambda_e \frac{\partial T}{\partial z} \right) - A = 0 \quad (2)$$

$$217 T(z_0, t) = T_{GS}(t) \quad (3)$$

$$218 \frac{\partial T}{\partial z} (z_{max}) = \frac{q_b}{\lambda_e} \quad (4)$$

219 where the index  $e$  marks effective properties that describe the rock–fluid two-phase system as  
 220 given by  $(\rho c)_e = \varphi \rho_w c_w + (1 - \varphi) \rho_m c_m$ , where the index of  $w$  and  $m$  represent water and matrix,  
 221 and  $\varphi$  represents porosity.  $q_b$  is the assumed basal heat flow at  $z_{max}$ .

222 To obtain a quantitative and stable GST history path, we performed a 1-D Tikhonov  
 223 deterministic method inversion and a Bayesian stochastic approach with a Metropolis-Hastings  
 224 Markov Chain Monte Carlo (MCMC) algorithm (code from  
 225 [https://github.com/volkerrath/BTI\\_2019](https://github.com/volkerrath/BTI_2019)) (Rath and Mottaghy, 2007; Rath et al., 2012). The  
 226 Tikhonov method estimated the GST history by a regularized least-squares procedure, with the  
 227 generalized cross-validation method's (GCV) optimum regularization parameter. The MCMC  
 228 inversion used the delayed rejection adaptive Monte Carlo (DRAM) algorithm (Haario et al.,  
 229 2006).

### 230 4.2 Input parameters

231 The input parameters for the model include the temperature log, thermal conductivity,  
 232 density, porosity, heat production (presented above), and matrix heat capacity (Zhu, 2011), along  
 233 with the current annual mean surface temperature of  $8^\circ\text{C}$ . Forward models were run for a 6000-  
 234 m profile to avoid potential boundary effects, whereas inverse models were run for the 60-600 m  
 235 interval, where an abnormally low heat flow implies a GST perturbation (as discussed above).  
 236 Models were run using a basal heat flow of  $78\text{-}80 \text{ mW m}^{-2}$ , similar to the average of observations  
 237 at depths of 600-1200 m, which is below the interval used for GST reconstruction.

238 **5 Results and Discussions**239 **5.1 Inversed GST history**

240 The Tikhonov method suggests a continuous and smoothed GST increase since 40-30 kyr  
 241 BP (Figure 4a). The MCMC inversion shows similar GST histories between 30 and 0.1 kyr BP,  
 242 based on  $4.0 \times 10^6$  samples, of which 29% were accepted. At earlier times, the modeling results of  
 243 the two methods are different. The inverted vertical temperature profile fits well with the  
 244 observed values, with temperature residuals smaller than 0.05 K (Figures 4b and 4c).

245 GST histories estimated using both methods show overall warming of approximately 10  
 246 K from approximately 20 kyr. We note the MCMC inversion results in several abrupt and  
 247 possibly excessive temperature changes of magnitude ~5 K on centennial to millennial time  
 248 scales at approximately 4-30 kyr BP. The Tikhonov inversion aims to derive one "optimum"  
 249 model, which may produce many equivalent models (Rath and Mottaghy, 2007; Mottaghy et al.,  
 250 2013), whereas MCMC methods yield a joint posterior distribution of the parameters.  
 251 Considering GST history inversions highlight only the low-frequency variability (Pollack et al.,  
 252 2006), the smooth Tikhonov inversions can reflect the past GST variations, probably better than  
 253 the variable MCMC results. Unless specified, the reconstructed GST in the following sections  
 254 refers to Tikhonov inversions.

255 The GST reconstructions for the period from 0.1-30 kyr BP are consistent with previous  
 256 studies. The use of temperature intervals at depths greater than 60 m means that our inversions  
 257 are not sensitized to GST changes over the last century. We note that the Tikhonov inversions  
 258 are consistent with the last five-century cumulative GST change of +2 K (Figure 4a), which is  
 259 consistent with the value in southeastern Australia (Beardsmore et al., 2017) and slightly larger  
 260 than the average of 1.1 K in the Northern Hemisphere (Huang et al., 2000). The results also  
 261 exhibit a 10 K GST rise from the minimum temperature during the Last Glacial Maximum,  
 262 which is consistent with the scientific drilling in Olkiluoto (Kukkonen et al., 2011), but lower  
 263 than those determined in northern Poland (~13 K) (Majorowicz and Safanda, 2008) and  
 264 northwestern Russia (12-13 K) (Demezhko and Shchapov, 2001).

265 The fact that the inversions diverge for periods greater than 30 kyr BP means that our  
 266 confidence in the GST histories before the Last Glacial Maximum is low. This may in part  
 267 reflect the impact of thermal effects of transient fluid migration in the deeper part of the section  
 268 modeled in GST inversions. Furthermore, because the top 40 m of the temperature log is likely  
 269 impacted by groundwater flow and seasonal temperature variations, these suggest the decreased  
 270 temperature in the last tens of years in both inversions is not considered reflective of climate  
 271 change.

272 **5.2 Uncertainties from local heat convection**

273 The inversions discussed above show that even in the presence of localized basin-scale  
 274 fluid movements, the borehole temperature can still record the past GST signals. The new  
 275 thermal equilibrium was reached after the stable and long-lasting fluid migrations. The heat  
 276 effect of fluid migration is equivalent to the lower boundary of variable heat flow. Furthermore,  
 277 most climate reconstruction boreholes are only a few hundred meters deep (Beltrami et al.,  
 278 2006), despite the recorded temperature period revealing little hydrologic activity, and the deeper  
 279 interval is uncertain. Local fluid activity may exist in most circumstances. The local fluid  
 280 convection beneath the recorded maximum depth (particularly far from the borehole bottom)

would not erase the GST history signals, as shown by the consistency among the GST reconstructions (Vogt et al., 2014; Beltrami et al., 2017; Erkan et al., 2019). To further validate the above discussion, parameter numerical simulation experiments were conducted. The thermal effect of fluid activity was equivalent to a sharp increase in temperature at the corresponding depth, forming a temperature field, which was then used as input for inversion. The results showed that assuming a  $\pm 5$  K groundwater temperature change at depths below 1 km, the inverted temperature rise varies between 8 K and 12 K since 20 kiloyear BP. This result remains consistent with this and previous studies (see Supplementary Materials for details). Although utilizing thermo-hydro modeling would be helpful in testing and removing the effects of fluid convection (Vogt et al., 2014), it requires far more computational resources and involves more uncertainties in additional hydraulic parameters for modeling the fluid flow.

### 5.3 Affecting heat flow estimate

The aforementioned result also serves as a reminder for utilizing caution when determining heat-flow data from shallow boreholes. The borehole depths should be taken into account when analyzing the heat-flow distribution, particularly for sedimentary basins. For instance, advective fluid flow and paleoclimate mask the deep heat-flow signal, as shown by the increasing trend of heat flow from the western to central areas of the Songliao Basin (Figure 1c). In this regard, the SK-2e shows the importance of superdeep boreholes in establishing criteria for discerning the relative contributions of these different factors to the observed temperature gradients and heat flow. A detailed analysis of the vertical variation in the heat flow has implications for obtaining high-quality heat-flow data to remove the effect of lateral convective heat and GST changes. The newly determined heat flow is consistent with the values determined from other deep boreholes penetrating the crystalline basement in eastern China (Figure 1a), including CCSD-MH, ( $\sim 66 \text{ mW m}^{-2}$  at 4600 m) (He et al., 2009), and borehole LZ ( $\sim 69 \text{ mW m}^{-2}$  at  $\sim 3500$  m) (Jiang et al., 2016). The consistency among the three heat-flow values implies that heat flow in eastern China is quite typical for a continental interior.

## 6. Conclusions

The equilibrium temperature log and thermal conductivity data yield a 6100-m vertical heat-flow profile in SK-2e. The lower section of the profile exhibits a representative background heat-flow value of  $66 \text{ mW m}^{-2}$  from 4000 to 6000 m, corresponding to a surface value of  $71 \text{ mW m}^{-2}$  when the  $\sim 5 \text{ mW m}^{-2}$  heat-production contribution in the upper layers is factored in. The heat-flow profile in the uppermost 600 m mostly recorded a 2 K rise of GST in the last five centuries (0.1-0.6 kyr BP) and a 10 K rise of GST since the Last Glacial Maximum ( $\sim 30\text{-}20$  kyr BP). These results also suggest that the paleoclimate effects have reduced the apparent heat-flow data measured in the uppermost 1 km by as much as  $10\text{-}20 \text{ mW m}^{-2}$ . Significant localized positive heat-flow anomalies within the deeper segments agree well with the identified high-porosity/permeability zones. A comparison of the surrounding vertical heat-flow profiles indicates that the heat-flow anomalies are regionally distributed in the Songliao Basin and can be attributed to differences in the advective heat transport. Our study not only emphasizes the importance of high-quality geothermal temperature logging data in reconstructing past climates but also reveals their potential for climate correction for heat-flow determinations.

322 **Acknowledgments**

323 This research is supported by the National Natural Science Foundation of China (No.:  
 324 42004076, 42130809, 41888101, and 42074096). We thank Professor Chengshan Wang for his  
 325 help during the temperature logging. Constructive reviews from Dr. Volker Rath and an  
 326 anonymous reviewer, and handling editor Dr. Harihar Rajaram clarified many points in this  
 327 manuscript.

328

329 **Open Research**

330 All the observation data are provided in supplementary materials Datasets S1 to S9 and are  
 331 available on FigShare (<https://doi.org/10.6084/m9.figshare.22273054.v3>).

332 **References:**

- 333 Beardmore, G. R., and J. P. Cull (2001), Crustal heat flow: a guide to measurement and  
 334 modelling, Cambridge University Press, UK, pp: 132-133.
- 335 Beardmore, G., M. Sandiford, K. Gordon, M. Mclean, and S. McLaren (2017), Heat flow and  
 336 inferred ground surface temperature history at Tynong North, southeastern Australia,  
 337 Australian Journal of Earth Sciences, 64(6), 1-15.
- 338 Birch, F. (1954), Heat from radioactivity, Nuclear geology, 8, 148-174.
- 339 Chen, T. (2018), The study of logging response characteristic and mechanism of ultra-deep  
 340 borehole core based on the Scientific Drilling in Songliao Basin, MA thesis, Jilin  
 341 University, Jilin, China (in Chinese).
- 342 Davies, J. H. (2013), Global map of solid Earth surface heat flow, *Geochemistry Geophysics  
 343 Geosystems*, 14(10), 4608-4622
- 344 Demeshko, D. Y., and V. A. Shchapov (2001), 80,000 years ground surface temperature history  
 345 inferred from the temperature-depth log measured in the superdeep hole SG-4 (the Urals,  
 346 Russia), *Global & Planetary Change*, 29(3-4), 230.
- 347 Deng, C. L., H. Y. He, Y. X. Pan, and R. X. Zhu (2013), Chronology of the terrestrial Upper  
 348 Cretaceous in the Songliao Basin, northeast Asia, *Palaeogeography Palaeoclimatology  
 349 Palaeoecology*, 385, 44-54.
- 350 Erkan, K., B. Akkoyunlu, M. O. Inal, E. Balkan-Pazvantoglu, and M. Tayanc (2019), Twentieth-  
 351 century paleoclimatic modeling of borehole temperatures in western and central Anatolia  
 352 regions, Turkey, *International Journal of Earth Sciences*, 108(4), 1137-1146.
- 353 Furlong, K. P., and D. S. Chapman (2013), Heat Flow, Heat Generation, and the Thermal State  
 354 of the Lithosphere, *Annual Review of Earth and Planetary Sciences*, 41, 385-410.
- 355 Gosnold, W., J. Majorowicz, R. Klenner, and S. Hauck (2011), Implications of Post-Glacial  
 356 Warming for Northern Hemisphere Heat Flow, *Grc Transactions*, 35, 14-19.
- 357 Guillou-Frottier, L., C. Carré, B. Bourgine, V. Bouchot, and A. Genter (2013), Structure of  
 358 hydrothermal convection in the Upper Rhine Graben as inferred from corrected  
 359 temperature data and basin-scale numerical models, *Journal of Volcanology and  
 360 Geothermal Research*, 256, 29-49.

- 361 Haario, H., M. Laine, A. Mira, and E. Saksman (2006), DRAM: Efficient adaptive MCMC,  
362 Statistics & Computing, 16(4), 339-354.
- 363 He, L., S. Hu, W. Yang, and J. Wang (2009), Radiogenic heat production in the lithosphere of  
364 Sulu ultrahigh-pressure metamorphic belt, Earth and Planetary Science Letters, 277(3–4),  
365 525-538.
- 366 Huang, S., H. N. Pollack, and P. Shen (2000), Temperature trends over the past five centuries  
367 reconstructed from borehole temperatures, Nature, 403(6771), 756-758.
- 368 Jessop, A. M. (1987), Estimation of lateral water flow in an aquifer by thermal logging,  
369 Geothermics, 16(2), 117-126.
- 370 Jessop, J. A. M. A. (1993), Relation between basement heat flow and thermal state of the  
371 sedimentary succession of the Alberta Plains, Bulletin of Canadian Petroleum Geology,  
372 41(3), 358-368.
- 373 Jiang, G., X. Tang, S. Rao, P. Gao, L. Zhang, P. Zhao, and S. Hu (2016), High-quality heat flow  
374 determination from the crystalline basement of the south-east margin of North China  
375 Craton, Journal of Asian Earth Sciences, 118, 1-10.
- 376 Jiang, G., S. Hu, Y. Shi, C. Zhang, Z. Wang, and D. Hu (2019), Terrestrial heat flow of  
377 continental China: Updated dataset and tectonic implications, Tectonophysics, 753, 36-  
378 48.
- 379 Kappelmeyer, O., and R. Haenel (1974), Geothermics with special reference to application,  
380 Geoexploration Monographs Series 4, Gebrueder Borntraeger, Berlin.
- 381 Kukkonen, I. T., V. Rath, L. Kivek S, J. Afanda, and V. Ermak (2011), Geothermal studies of the  
382 Outokumpu Deep Drill Hole, Finland: Vertical variation in heat flow and palaeoclimatic  
383 implications, Physics of the Earth and Planetary Interiors, 188(1–2), 9-25.
- 384 Majorowicz, J., and J. Safanda (2008), Heat flow variation with depth in Poland: evidence from  
385 equilibrium temperature logs in 2.9-km-deep well Torun-1, International Journal of Earth  
386 Sciences, 97(2), 307-315.
- 387 Majorowicz, J., W. Gosnold, A. Gray, J. Safanda, R. Klenner, and M. Unsworth (2012),  
388 Implications of Post-Glacial Warming for Northern Alberta Heat Flow-Correcting for the  
389 Underestimate of the Geothermal Potential, GRC Transactions, 36, 693-698.
- 390 Mottaghy, D., R. Schellschmidt, Y. A. Popov, C. Clauser, I. T. Kukkonen, G. Nover, S.  
391 Milanovsky, and R. A. Romushkevich (2005), New heat flow data from the immediate  
392 vicinity of the Kola super-deep borehole: Vertical variation in heat flow confirmed and  
393 attributed to advection, Tectonophysics, 401(1-2), 119-142.
- 394 Mottaghy, D., G. Schwamborn, and V. Rath (2013), Past climate changes and permafrost depth  
395 at the Lake El'gygytgyn site: implications from data and thermal modeling, Climate of  
396 the Past, 9(1), 119-133.
- 397 Pollack, H. N., Nathenson, M., and M. Guffanti (1988), Geothermal Gradients in the  
398 Conterminous United States, Journal of Geophysical Research. Part B: Solid Earth, 93(6),  
399 6437-6450.

- 400 Pollack, H. N., S. Huang, and J. E. Smerdon (2006), Five centuries of climate change in  
 401 Australia: the view from underground, *Journal of Quaternary Science*, 21(7), 701-706.
- 402 Popov, Y. A., D. Pribnow, J. H. Sass, C. F. Williams, and H. Burkhardt (1999), Characterization  
 403 of rock thermal conductivity by high-resolution optical scanning, *Geothermics*, 28(2),  
 404 253-276.
- 405 Rath, V., and D. Mottaghy (2007), Smooth inversion for ground surface temperature histories:  
 406 estimating the optimum regularization parameter by generalized cross-validation,  
 407 *Geophysical Journal of the Royal Astronomical Society*, 171(3), 1440-1448.
- 408 Rath, V., J. F. González Rouco, and H. Goosse (2012), Impact of postglacial warming on  
 409 borehole reconstructions of last millennium temperatures, *Climate of the Past*, 8(3), 1059-  
 410 1066.
- 411 Sekiguchi, K. (1984), A method for determining terrestrial heat flow in oil basinal areas,  
 412 *Tectonophysics*, 103(1-4), 67-79.
- 413 Shi, Y., G. Jiang, X. Zhang, Z. Yuan, Z. Wang, Q. Qiu, and S. Hu (2018), Present temperature  
 414 field characterization and geothermal resource assessment in the Harbin Area, Northeast  
 415 China, *Energy Exploration & Exploitation*, 54861490.
- 416 Vogt, C., D. Mottaghy, V. Rath, G. Marquart, L. Dijkshoorn, A. Wolf, and C. Clauser (2014),  
 417 Vertical variation in heat flow on the Kola Peninsula: palaeoclimate or fluid flow?  
 418 *Geophysical Journal International*, 199(2), 829-843.
- 419 Wang, C., Z. Feng, L. Zhang, Y. Huang, K. Cao, P. Wang, and B. Zhao (2013), Cretaceous  
 420 paleogeography and paleoclimate and the setting of SKI borehole sites in Songliao Basin,  
 421 northeast China, *Palaeogeography, Palaeoclimatology, Palaeoecology*, 385, 17-30.
- 422 Wang, P., F. Mattern, N. A. Didenko, D. Zhu, B. Singer, and X. Sun (2016), Tectonics and cycle  
 423 system of the Cretaceous Songliao Basin: An inverted active continental margin basin,  
 424 *Earth-Science Reviews*, 159, 82-102.
- 425 Wu, Q. F., and Xie, Y. Z. (1985), Geothermal heat flow in the Songhuajiang-Liaoning Basin,  
 426 *Seismology and Geology*, 7(02), 59-64 (in Chinese).
- 427 Zhu, H. L. (2011), Research on the sedimentary geothermal resources in North Songliao Basin,  
 428 Ph.D. thesis, Northeast Petroleum University, Daqing, China (in Chinese).
- 429 Zou, C., Zhang, X., Zhao, J., Peng, C., Zhang, S., Li, N., Xiao, L., Niu, Y., Ding, Y., Qin, Y.,  
 430 and Lin, F. (2018), Scientific Results of Geophysical Logging in the Upper Cretaceous  
 431 Strata, CCSD SK-2 East Borehole in the Songliao Basin of Northeast China, *Acta  
 432 Geoscientica Sinica*, 39(06), 679-690 (in Chinese).
- 433 Zschocke, A., V. Rath, C. Grissemann, and C. Clauser (2005), Quantifying deep fluid flow in  
 434 inclined reservoirs from correlated discontinuities in vertical heat flow, *Journal of  
 435 Geophysics and Engineering*, 2, 232-242.
- 436
- 437 **References cited in the online supporting information**
- 438 Carslaw, H. S., and J. C. Jaeger (1959), *Conduction of Heat in Solids*, Oxford University Press,  
 439 USA, pp: 99.

- 440 Su, Y. (2021), Genesis and rational development of typical geothermal field in the Songliao  
441 Basin: a case study of Lindian geothermal field, Ph.D. thesis, Jinlin University,  
442 Changchun (in Chinese).  
443  
444

445 **Figure captions**

446 **Figure 1.** (a) Tectonic setting and topography surrounding SK-2e. (b) Subunits of the Songliao  
 447 Basin, location of SK-2e, and previous heat-flow measurements (Wu and Xie, 1985). SK-1n and  
 448 N2 are complementary core samples. The CCSD-MH (Chinese Continental Scientific Drilling  
 449 Main Hole) and LZ show the location of the previous continuous heat-flow profile penetrating  
 450 the crystalline basement. (c) Stratigraphic cross-section of AA', interpreted with borehole-  
 451 constrained seismic data (modified from Wang et al. (2013)), and simplified vertical heat-flow  
 452 profile along the cross-section. Heat flows that are higher and lower than the background value  
 453 of  $70 \text{ mW m}^{-2}$  are filled in red and blue, respectively. Formation symbols: K<sub>1</sub>h=Huoshiling,  
 454 K<sub>1</sub>s=Shahezi, K<sub>1</sub>y=Yingcheng, K<sub>1</sub>d=Denglouku, K<sub>2</sub>q=Quantou, K<sub>2</sub>qn=Qingshankou,  
 455 K<sub>2</sub>y=Yaojia, K<sub>2</sub>n=Nenjiang, K<sub>2</sub>s=Sifangtai, K<sub>2</sub>m=Mingshui, and Q=Quaternary (Deng et al.,  
 456 2013).

457 **Figure 2.** (a) Temperature log at 35 days after drilling that stopped halfway in 2016 and 507  
 458 days after drilling that finished in 2019. (b) Temperature gradient at 20-m intervals. (c) Heat  
 459 flow vertical variations. The red stepped line is the arithmetic mean of the temperature  
 460 gradient/heat flow data of each segment. The shaded area is the  $\pm 1$  standard deviation (SD). The  
 461 cyan line is the linear least squares smoothed temperature gradient and heat flow in the 100-m  
 462 interval.

463 **Figure 3.** (a) Thermal conductivity, (b) U-Th-K concentration, (c) heat production, (d) porosity  
 464 and permeability, (e) heat flow, and (f) stratigraphic column of SK-2e. The different colored  
 465 spots in (c) present the rock types as in (f).

466 **Figure 4.** Tikhonov inversions and MCMC inversions of the SK-2e geothermal data in 60-600 m  
 467 intervals. (a) Estimated GST history using the Tikhonov and MCMC inversion methods. (b) and  
 468 (c) Temperature residuals of Tikhonov and MCMC inversions.

469  
 470

**Figure 1.**

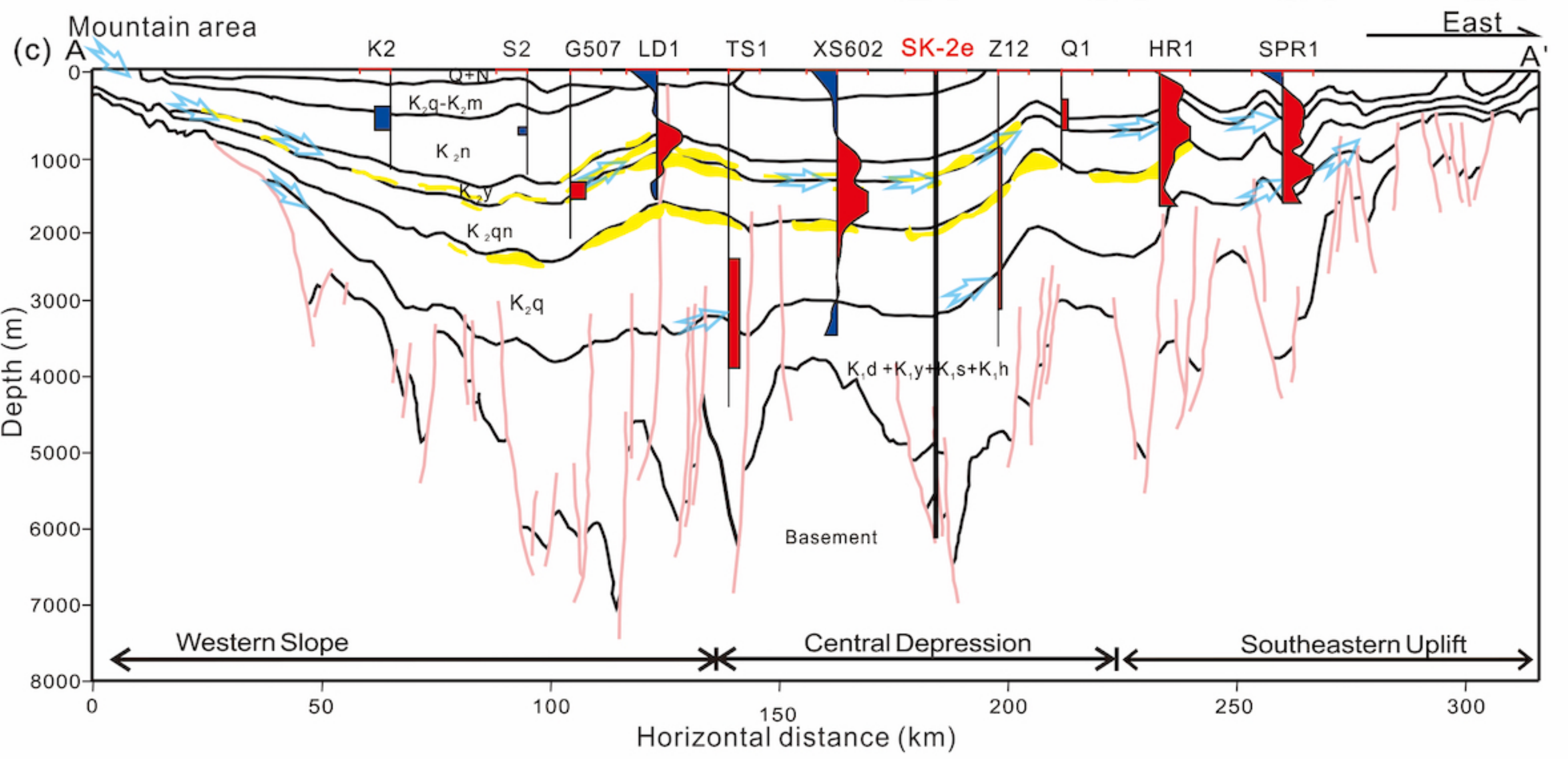
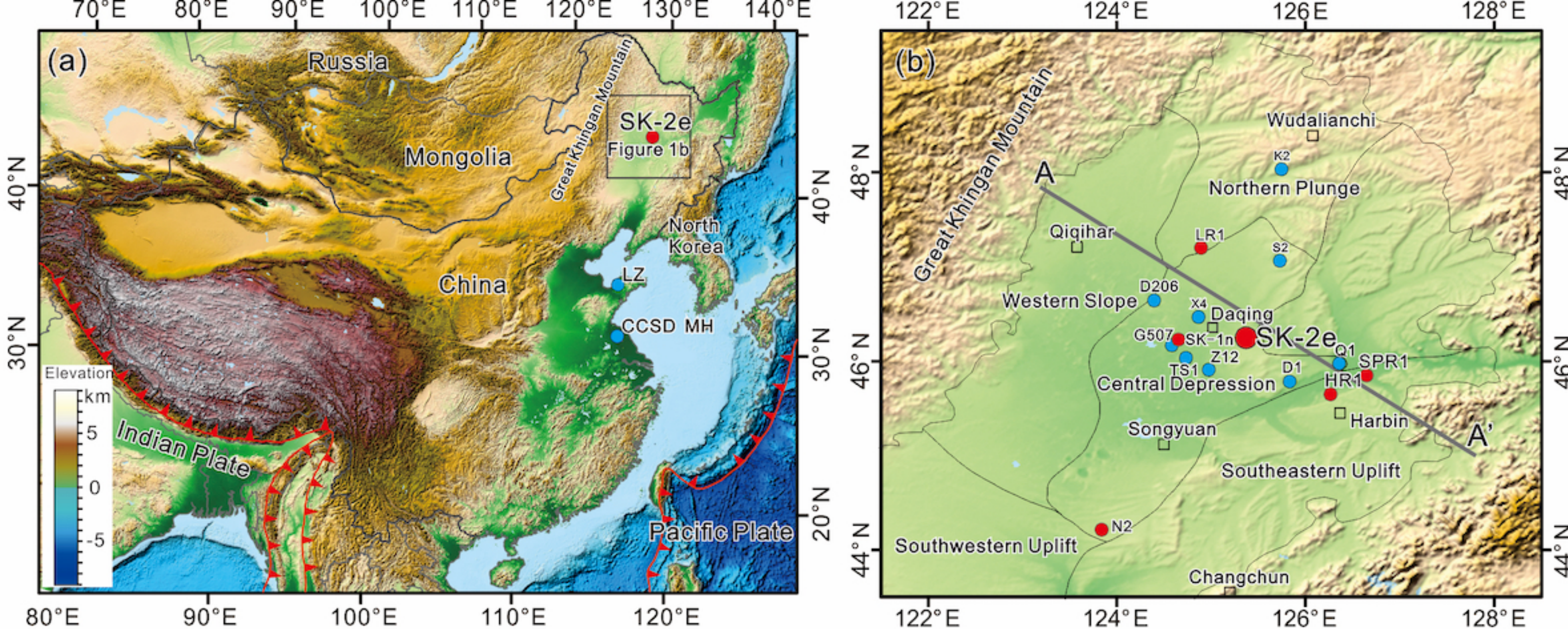


**Figure 2.**

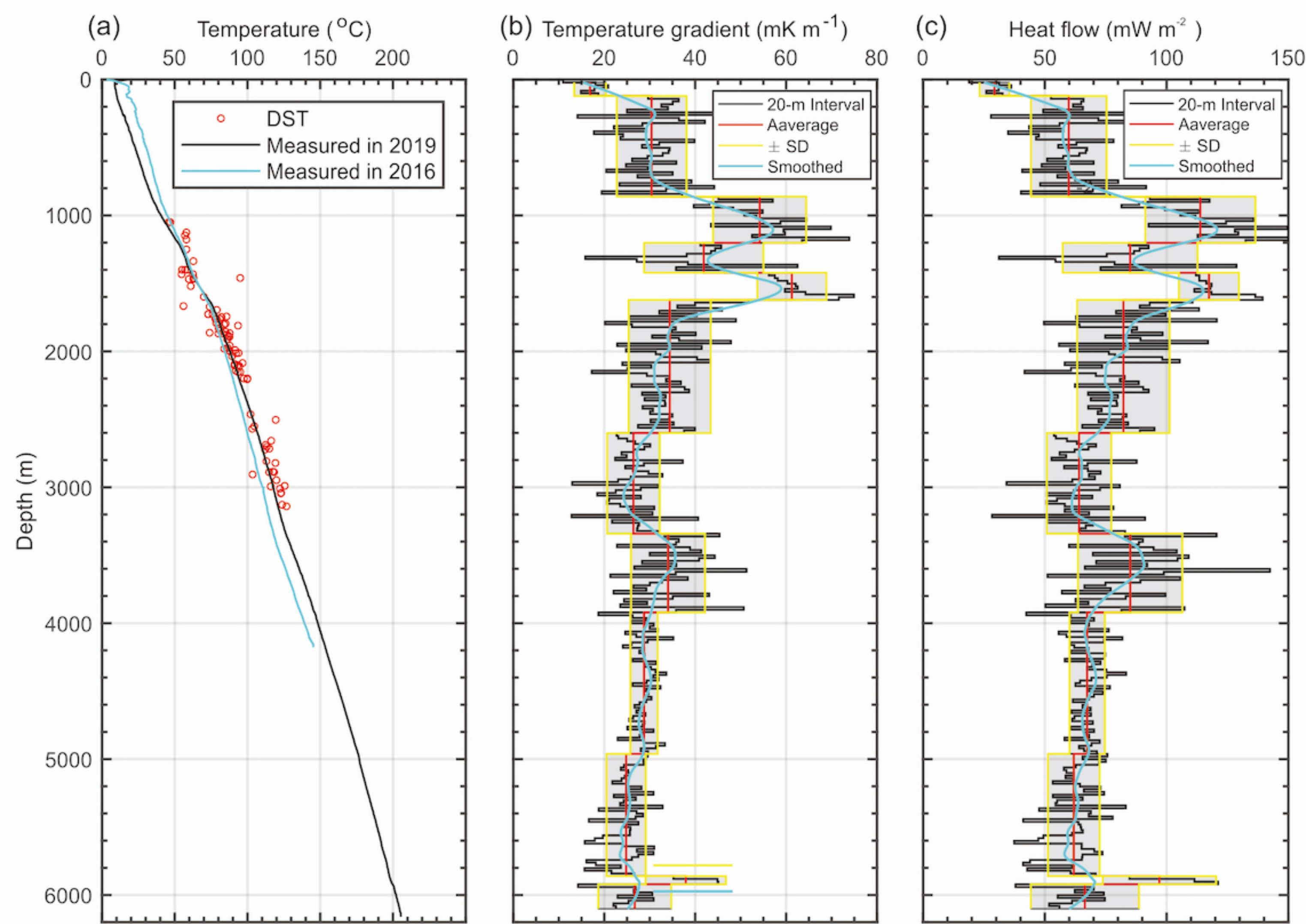


**Figure 3.**

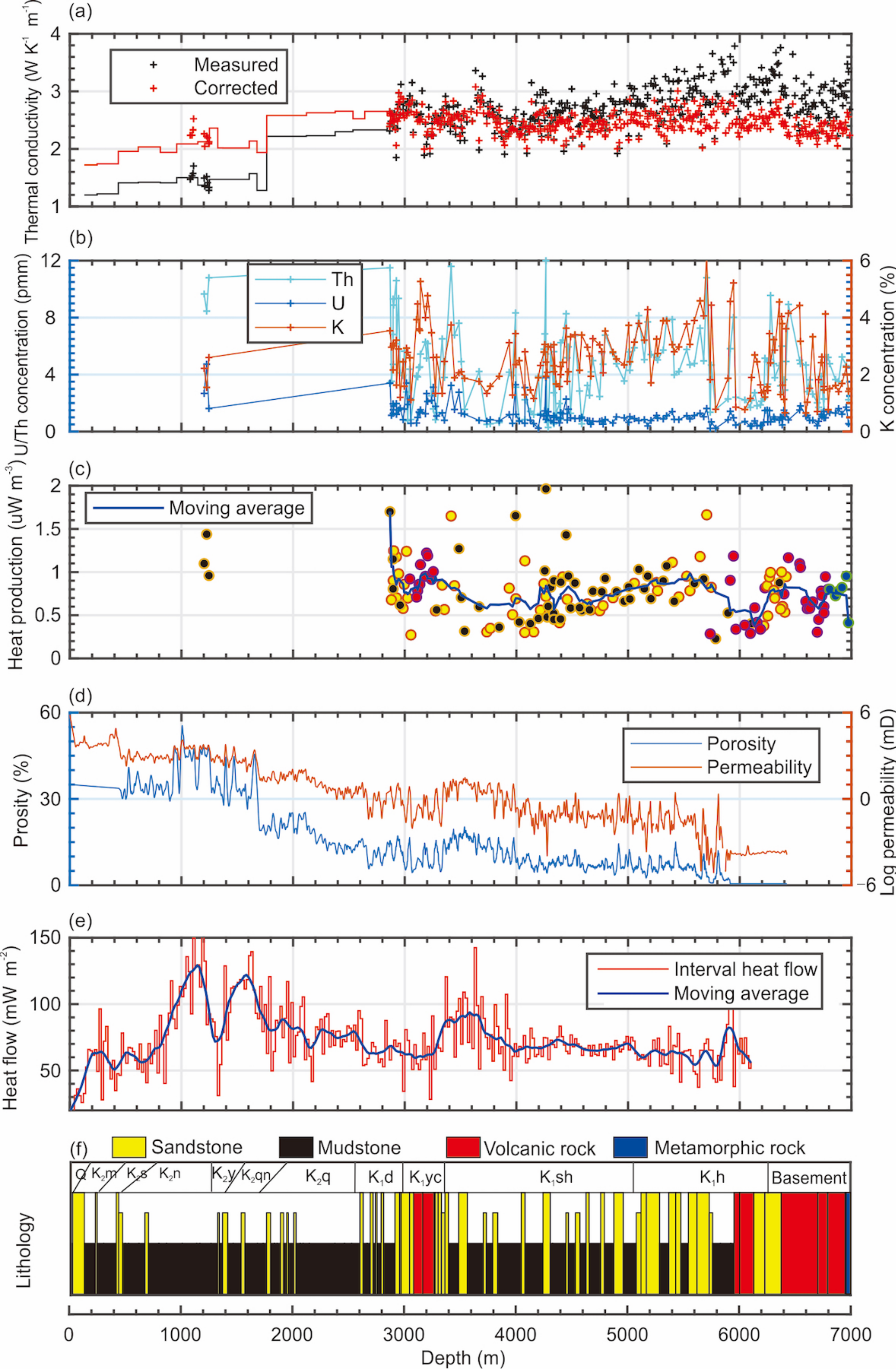


**Figure 4.**

